RESEARCH ARTICLE SUMMARY

CELL BIOLOGY

The human disease gene LYSET is essential for lysosomal enzyme transport and viral infection

Christopher M. Richards, Sabrina Jabs, Wenjie Qiao, Lauren D. Varanese, Michaela Schweizer, Peter R. Mosen, Nicholas M. Riley, Malte Klüssendorf, James R. Zengel, Ryan A. Flynn, Arjun Rustagi, John C. Widen, Christine E. Peters, Yaw Shin Ooi, Xuping Xie, Pei-Yong Shi, Ralf Bartenschlager, Andreas S. Puschnik, Matthew Bogyo, Carolyn R. Bertozzi, Catherine A. Blish, Dominic Winter, Claude M. Nagamine, Thomas Braulke*, Jan E. Carette*

INTRODUCTION: Lysosomes are key degradative compartments within the cell that are essential to maintain protein homeostasis. Their dysfunction causes over 70 rare genetic diseases collectively known as lysosomal storage disorders (LSDs). Intracellular sorting of most soluble lysosomal enzymes occurs by tagging with mannose 6-phosphate (M6P) residues in the Golgi apparatus, which are recognized by specific receptors that direct transport to the endosomal/lysosomal system. GlcNAc-1-phosphotransferase catalyzes the first step in M6P-tagging. Inherited loss of GlcNAc-1-phosphotransferase function causes the severe LSD mucolipidosis type II (MLII). The M6P signal-mediated lysosomal sorting pathway is well studied and thought to be completely understood. However, it remains unknown whether additional critical components exist.

RATIONALE: Certain viruses program successful entry into cells by co-opting lysosomal cathepsin proteases to cleave and activate viral structural proteins allowing delivery of their genome into the cytoplasm. This infection strategy is shared among different virus families including reovirus, Ebola virus, and severe acute respiratory syndrome coronavirus 2 (SARS-CoV-2). Therefore, these viruses are sensitive probes for lysosomal function. To identify genes important for lysosomal homeostasis, we performed genome-scale CRISPR screens using susceptibility to reovirus infection as phenotypic selection.

RESULTS: The genetic screens identified TMEM251—a small, uncharacterized protein—as an essential component of lysosomal biogenesis. Cells with knockout (KO) mutations in TMEM251 were refractory to infection by reovirus, SARS-CoV-2, and vesicular stomatitis virus pseudotyped with the Ebola virus glycoprotein. This was due to strongly reduced activity of lysosomal cathepsin proteases. Moreover, quantitative proteomics revealed a severe global sorting defect in which intracellular enzymes destined for lysosomal delivery were instead secreted into the medium. Thus, we renamed TMEM251 to LYSET (for lysosomal enzyme trafficking factor). Mechanistically, we showed that LYSET binds to GlcNAc-1-phosphotransferase in the Golgi apparatus and controls its stability. LYSET KO caused aberrant localization of GlcNAc-1-phosphotransferase to lysosomes and subsequent degradation, resulting in M6P tagging failure. LYSET KO mice displayed typical diagnostic features of MLII including elevated levels of lysosomal enzymes in blood serum and enlarged lysosomes with accumulation of electron dense material in isolated cells. Recently, an MLII-like genetic disorder in patients carrying biallelic mutations in LYSET has been described. We showed that complementation of LYSET KO cells with these pathogenic mutants failed to rescue lysosomal sorting defects.

CONCLUSION: Our work identifies LYSET as an indispensable component of the biosynthetic pathway that directs transport of soluble enzymes to the lysosome. As such, LYSET is essential for entry of diverse, highly pathogenic viruses that rely on endo-lysosomal activation by cathepsins. We uncovered an unexpected molecular mechanism in which LYSET regulates GlcNAc-1-phosphotransferase function by binding to and retaining it in the Golgi apparatus. The key role of LYSET in lysosome biogenesis likely explains MLII-like symptoms observed in patients with LYSET mutations. Altogether, our findings provide insights in fundamental cell physiology with relevance for human inherited disease and viral infection. ■

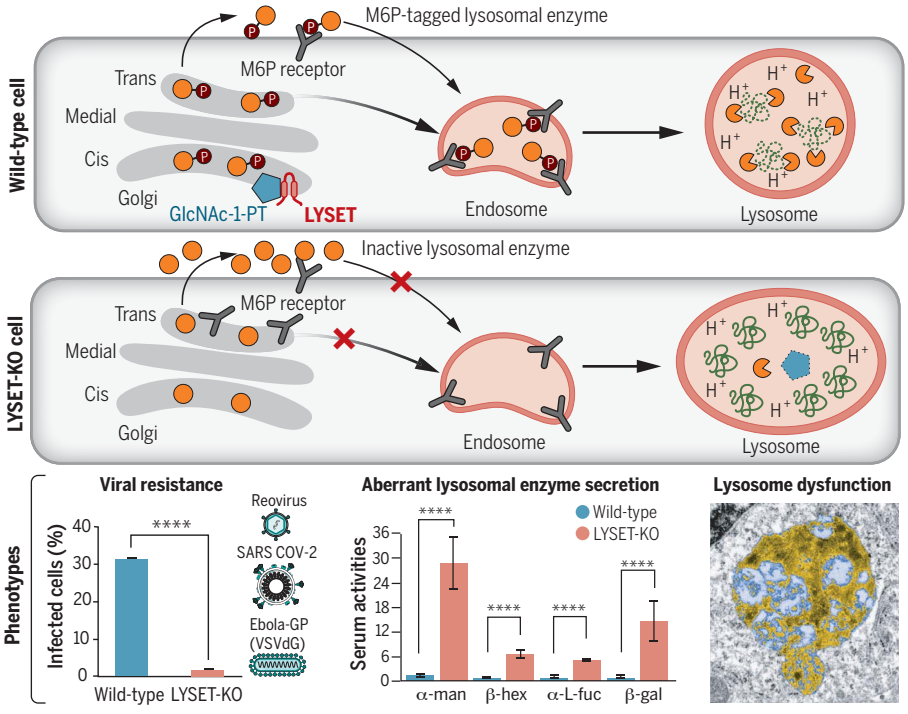

LYSET is an essential component of the M6P lysosomal transport pathway. By using genome-scale genetic screens for viral infection we identified LYSET as a protein required for lysosome biogenesis. LYSET controls GlcNAc-1-phosphotransferase (GlcNAc-1-PT) function by binding to and retaining it in the Golgi apparatus. In LYSET KO cells M6P tagging is severely disrupted resulting in strong resistance to infection by certain viruses, aberrant secretion of enzymes normally present in the lysosome, and abnormally large lysosomes filled with storage material as a result of drastically reduced levels of active hydrolytic enzymes.

The list of author affiliations is available in the full article online.
*Corresponding author. Email: braulke@uke.de (T.B.); carette@stanford.edu (J.E.C.)
Cite this article as C. M. Richards *et al.*, *Science* **378**, eabn5648 (2022). DOI: 10.1126/science.abn5648

READ THE FULL ARTICLE AT
https://doi.org/10.1126/science.abn5648

RESEARCH ARTICLE

CELL BIOLOGY

The human disease gene LYSET is essential for lysosomal enzyme transport and viral infection

Christopher M. Richards[1]†, Sabrina Jabs[2]†, Wenjie Qiao[1]†, Lauren D. Varanese[1], Michaela Schweizer[3], Peter R. Mosen[4], Nicholas M. Riley[5], Malte Klüssendorf[6], James R. Zengel[1], Ryan A. Flynn[7,8], Arjun Rustagi[9], John C. Widen[10], Christine E. Peters[1], Yaw Shin Ooi[11], Xuping Xie[12], Pei-Yong Shi[12], Ralf Bartenschlager[13,14], Andreas S. Puschnik[15], Matthew Bogyo[1,10], Carolyn R. Bertozzi[5,16], Catherine A. Blish[9], Dominic Winter[4], Claude M. Nagamine[17], Thomas Braulke[6]*, Jan E. Carette[1]*

Lysosomes are key degradative compartments of the cell. Transport to lysosomes relies on GlcNAc-1-phosphotransferase–mediated tagging of soluble enzymes with mannose 6-phosphate (M6P). GlcNAc-1-phosphotransferase deficiency leads to the severe lysosomal storage disorder mucolipidosis II (MLII). Several viruses require lysosomal cathepsins to cleave structural proteins and thus depend on functional GlcNAc-1-phosphotransferase. We used genome-scale CRISPR screens to identify lysosomal enzyme trafficking factor (LYSET, also named TMEM251) as essential for infection by cathepsin-dependent viruses including severe acute respiratory syndrome coronavirus 2 (SARS-CoV-2). LYSET deficiency resulted in global loss of M6P tagging and mislocalization of GlcNAc-1-phosphotransferase from the Golgi complex to lysosomes. *Lyset* knockout mice exhibited MLII-like phenotypes, and human pathogenic LYSET alleles failed to restore lysosomal sorting defects. Thus, LYSET is required for correct functioning of the M6P trafficking machinery and mutations in LYSET can explain the phenotype of the associated disorder.

Viruses have evolved to hijack the cellular endocytic machinery to enter the cell (*1*). Lysosomal cathepsin proteases mediate the stepwise proteolytic disassembly of reovirus particles, which is essential for infection (*2*). Cathepsins also cleave viral glycoproteins of several enveloped viruses during viral entry, triggering productive infection. This includes highly pathogenic viruses including the filovirus family member Ebola virus (EBOV) and coronaviruses including severe acute respiratory syndrome coronavirus (SARS-CoV), SARS-CoV-2, and Middle East respiratory syndrome (MERS) coronaviruses (*3*–*6*). These viruses are thus sensitive probes of lysosomal function.

[1]Department of Microbiology and Immunology, Stanford University School of Medicine, Stanford, CA, USA. [2]Institute of Clinical Molecular Biology, Christian-Albrechts-University and University Medical Center Schleswig-Holstein, Campus Kiel, Kiel, Germany. [3]Department of Electron Microscopy, Center for Molecular Neurobiology, University Medical Center Hamburg-Eppendorf, Hamburg, Germany. [4]Institute for Biochemistry and Molecular Biology, Medical Faculty, Rheinische Friedrich-Wilhelms-University of Bonn, Bonn, Germany. [5]Department of Chemistry, Stanford University, Stanford, CA, USA. [6]Department of Osteology and Biomechanics, Cell Biology of Rare Diseases, University Medical Center Hamburg-Eppendorf, Hamburg, Germany. [7]Stem Cell Program, Boston Children's Hospital, Boston, MA, USA. [8]Stem Cell and Regenerative Biology Department, Harvard University, Cambridge, MA, USA. [9]Division of Infectious Disease and Geographic Medicine, Department of Medicine, Stanford University School of Medicine, Stanford, CA, USA. [10]Department of Pathology, Stanford University School of Medicine, Stanford, CA, USA. [11]Programme in Emerging Infectious Diseases, Duke-NUS Medical School, Singapore, Singapore. [12]Department of Biochemistry and Molecular Biology, University of Texas Medical Branch, Galveston, TX, USA. [13]Department of Infectious Diseases, Molecular Virology, Heidelberg University, Heidelberg, Germany. [14]Division Virus-Associated Carcinogenesis, German Cancer Research Center (DKFZ), Heidelberg, Germany. [15]Chan Zuckerberg Biohub, San Francisco, CA, USA. [16]Howard Hughes Medical Institute, Stanford, CA, USA. [17]Department of Comparative Medicine, Stanford University School of Medicine, Stanford, CA, USA.
***Corresponding author. Email: braulke@uke.de (T.B.); carette@stanford.edu (J.E.C.)**
†These authors contributed equally to this work.

LYSET is a cellular factor essential for infection by diverse viruses including SARS-CoV-2

To identify genes critical for reovirus infection, we performed a genome-scale CRISPR–Cas9 screen in human glioblastoma cells (U87MG). In these cells, productive viral infection leads to cell death. After CRISPR-Cas9 mutagenesis with the Brunello library (*7*), which covers 19,114 genes, cells were infected with reovirus type 3D (ReoT3D). To identify protective gene mutations, we retrieved the guide RNA (gRNA) sequences present in the resistant population and compared them with the unselected population (fig. S1A). In line with its essential role in reovirus entry, the gene encoding cathepsin L was highly enriched in the resistant population (Fig. 1A and table S1) (*8*). Consistent with the importance of mannose 6-phosphate (M6P)–dependent lysosomal transport for cathepsin activity (*9*), genes encoding the α/β (*GNPTAB*) (*10*) and γ (*GNPTG*) (*11*) subunits of GlcNAc-1-phosphotransferase scored highly, as did site-1 protease (S1P), a Golgi-localized protein required for the activation of GlcNAc-1-phosphotransferase (*12*). We did not identify M6P receptors (MPR), likely owing to functional overlap between the two M6P receptor types, cation-dependent and cation-independent MPR (*13*). The second highest hit was TMEM251, a gene encoding a largely uncharacterized transmembrane protein. Based on the results outlined below, we renamed this gene lysosomal enzyme trafficking factor (LYSET). A separate genome-scale CRISPR screen in eHAP cells also identified deletion of *GNPTAB* and *LYSET* as highly protective against reovirus infection, corroborating the essentiality of M6P-mediated lysosomal protein sorting and LYSET for reovirus infection (fig. S1B and table S2). To validate and characterize the role of LYSET, GNPTAB, and S1P in viral infection, we generated clonal knockout (KO) cell lines in U87MG and 293FT cells using CRISPR-Cas9 (fig. S2). Knockout of LYSET, GNPTAB, and S1P resulted in strong protection against cell death following reovirus infection in both cell types (Fig. 1B). Intracellular viral RNA levels and virus production were severely reduced, suggesting an early block in viral entry or replication (Fig. 1, C and D). Because GNPTAB, GNPTG, and S1P have known roles in the sorting of lysosomal cathepsins, we reasoned that LYSET might act similarly. We first tested whether LYSET deficiency would prevent viral entry of other cathepsin-dependent viruses (*3*). As a faithful model of EBOV entry (*14*) we used a GFP-encoding vesicular stomatitis virus pseudotyped with the EBOV glycoprotein (VSV-EBOV-GP). Whereas parental 293FT cells were susceptible to infection with VSV-EBOV-GP as evidenced by a time-dependent increase in GFP fluorescence, LYSET KO cells were highly refractory to infection (Fig. 1E, fig. S3A, and movies S1 and S2). Similar results were obtained using clonal HAP1 LYSET KO cells and pooled knockouts in human skin fibroblasts (fig. S3, B to D, and movies S3 to S6). SARS-CoV-2 requires activation of its spike protein during viral entry, which can be mediated by active endosomal or lysosomal cathepsins or by the transmembrane serine protease TMPRSS2 (*5*). In cells with very low TMPRSS2 expression, cathepsins become essential for SARS-CoV-2 entry. Whereas parental A549-ACE2 cells were highly susceptible to infection by VSV pseudotyped with the SARS-CoV-2 spike protein, deletion of LYSET strongly reduced infection levels during the time course of infection (fig. S3, E and F, and movies S7 and S8). To validate these results in the context of the authentic virus, we used an infectious molecular clone of SARS-CoV-2 that expresses the mNeonGreen fluorescent protein (*15*). Consistent with the results of the pseudotyped viruses, we observed a substantial decrease in infection (Fig. 1F and fig. S3G). In cells expressing TMPRSS2, most SARS-CoV-2 variants preferentially use this route of entry (*16*). However, the recently emerging omicron variant is less efficiently cleaved by TMPRSS2 and more dependent on cathepsin-mediated entry than other variants of concern such as the delta variant (*16*, *17*). We thus tested lentiviral particles

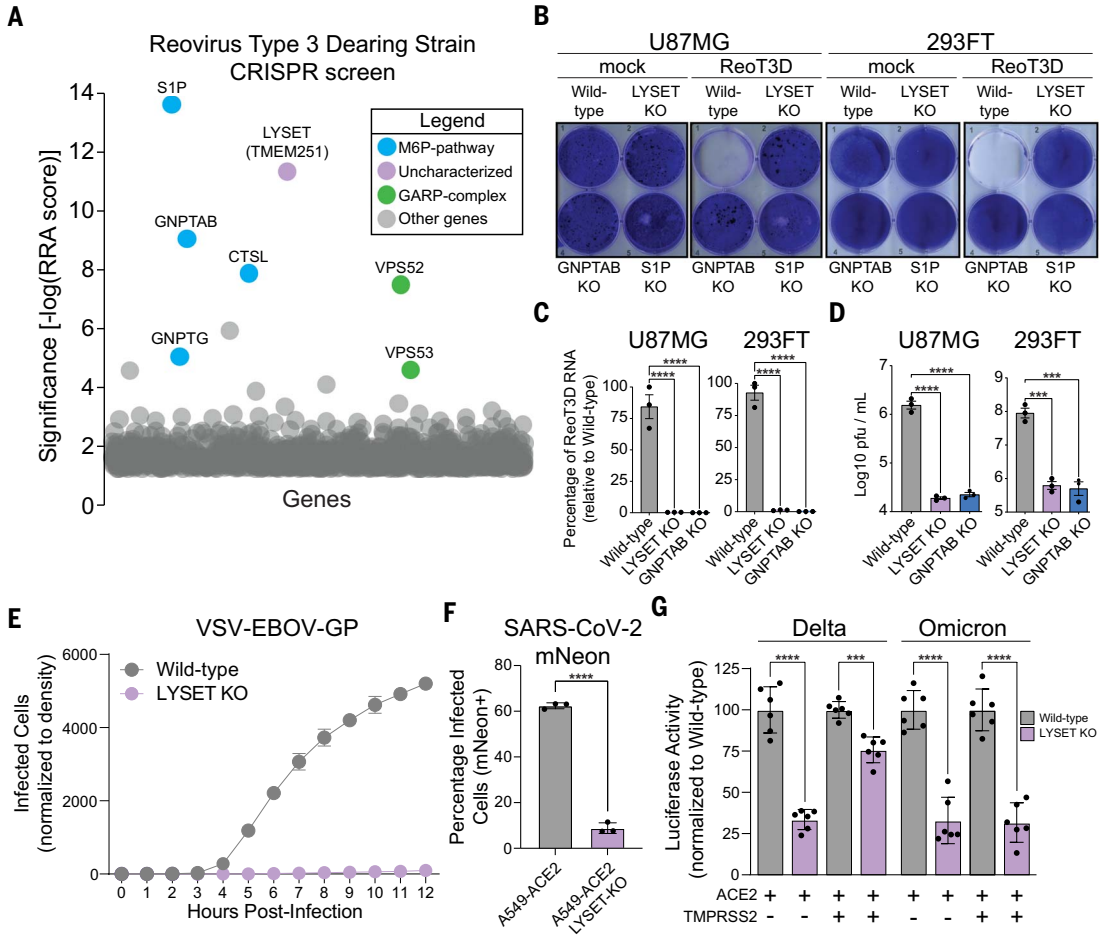

Fig. 1. LYSET is a critical host factor for multiple viruses that use activated cathepsins for entry. (**A**) CRISPR screen for reovirus T3D (ReoT3D) host factors in U87MG cells. Significance of enrichment was determined through MAGeCK analysis (*y* axis). All genes are plotted as bubbles on the *x* axis, each representing a specific gene. Each subset is color-coded according to function and labels show gene names. (**B**) Crystal violet staining after infection with ReoT3D representative of $n = 3$ biologically independent replicates. mock, noninfected controls. (**C**) RT-qPCR quantification of ReoT3D RNA in infected U87MG and 293FT cells at multiplicity of infection (MOI) 1 at 72 hours post infection (hpi) (mean ± SEM, $n = 3$) (**D**) U87MG or 293FT cells were infected with MOI of 1 ReoT3D virus. At 72 hpi, cells were lysed and viral titers determined through plaque assay [mean ± SEM, $n = 3$, $^{***}P < 0.001$, $^{****}P < 0.0001$; significance determined through one-way ANOVA with post-hoc Dunnett's multiple comparisons test for (**C**) and (**D**)]. (**E**) Time course of VSV-EBOV-GP infection of 293FT cells WT and LYSET KO (mean ± SEM, $n = 3$). (**F**) Bar graph depicting independent infections of A549-ACE2 cells ± LYSET KO with SARS-CoV-2-mNeon using flow cytometry (mean ± SD, $n = 3$, $^{****}P < 0.0001$; significance determined through unpaired, two-tailed student's t-test). (**G**) Infection of SARS-CoV-2 Delta and Omicron spike reporter virus particles in Huh7.5.1 cell lines with or without LYSET KO. Cells were engineered to stably express ACE2 or ACE2 in combination with TMPRSS2, as indicated. Luciferase activity was measured at 72 hpi and normalized to WT cells (mean ± SEM, $n = 6$, $^{***}P < 0.001$, $^{****}P < 0.0001$; significance was determined by unpaired, two-tailed student's t-test with Welch's correction).

pseudotyped with SARS-CoV-2 spike variants in cells that expressed or did not express TMPRSS2. Consistent with our results with spikes corresponding to the early Wuhan strain, LYSET KO resulted in decreased entry of both delta and omicron variant–pseudotyped viruses in cells that did not express TMPRSS2 (Fig. 1G). In cells expressing TMPRSS2, the delta variant was only moderately affected by LYSET KO whereas the omicron variant was still strongly dependent on LYSET (Fig. 1G). Thus, our genetic screens identified LYSET as a host factor essential for a diverse group of viruses that depend on endosomal protease activation during cell entry.

LYSET is critical for M6P-mediated lysosomal enzyme transport

The identification of a previously uncharacterized transmembrane protein potentially involved in cathepsin sorting was unexpected as the key proteins involved in lysosomal targeting are well established (*13*). To investigate whether LYSET affected lysosomal trafficking of cathepsins, we analyzed cathepsin B (CTSB) protein levels in 293FT and U87MG wild-type (WT) and KO cells (Fig. 2A and fig. S4A). In WT cells, most CTSB was present in its mature form following autocatalytic cleavage in lysosomes. Only low levels were found in the extracellular medium, indicating efficient lysosomal sorting and trafficking. By contrast, LYSET deficiency resulted in aberrant secretion of CTSB precursor forms into the medium concomitant with a near complete loss of mature CTSB in the cell lysate (Fig. 2A and fig. S4A). The dysregulation of cathepsin transport was equally pronounced as observed after disruption of core M6P formation components (GNPTAB and S1P). We extended the analysis to a larger panel of cathepsins in 293FT and HAP1 cells (fig. S4, B and C) and measured cathepsin activity using a quenched cell-permeable probe (BMV-109) that covalently links to active cysteine cathepsins and gains fluorescence (*18*). Compared with WT cells, LYSET KO cells displayed a

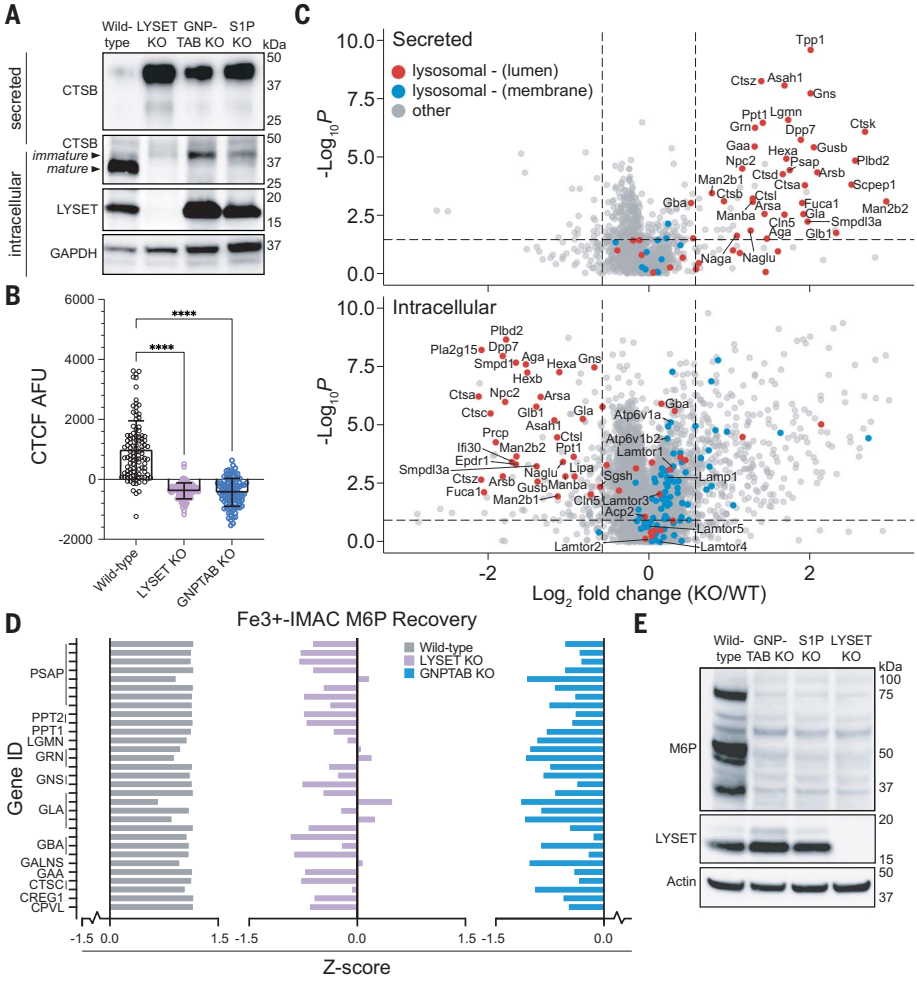

Fig. 2. LYSET is required for global lysosomal enzyme transport through M6P-tagging. (**A**) Immunoblot analysis of CTSB in lysates (intracellular) and in extracellular medium (secreted) from WT cells and clonal 293FT cell lines containing KO mutations in indicated genes. (**B**) Cathepsin activity in cells was determined by quantification of BMV-109 fluorescence signal in live 293FT WT and KO cells as the raw corrected total cellular fluorescence (CTCF) in arbitrary fluorescence units (AFU) (mean ± SD, n = 100 cells, ****P < 0.0001; significance determined through one-way ANOVA with a post-hoc Dunnett's multiple comparisons test). (**C**) Proteomic analysis of WT and LYSET KO MEFs by unbiased DIA. DIA was used for intracellular and secreted proteins. (**D**) Z-score analysis of individual peptides that contain the M6P moiety as determined using glycoproteomics. Peptides were derived from indicated lysosomal proteins in WT, LYSET KO, and GNPTAB KO 293FT cells; n = 3 replicates for each cell line. (**E**) Immunoblot analysis of M6P-tagged proteins from 293FT WT, GNPTAB KO, S1P KO, and LYSET KO cells using an M6P-specific, single-chain antibody fragment (M6P).

strongly decreased fluorescence after live cell labeling suggesting a global loss of cysteine cathepsin protease activity (Fig. 2B and fig. S4, D and E). This indicated a severe defect in lysosomal protein targeting because activity requires autocatalytic cleavage in lysosomes. To investigate whether the missorting was specific to cathepsins or pointed to a more general defect, we analyzed the consequences of LYSET deficiency for additional lysosomal proteins and in different cellular contexts. We consistently found large increases in secretion of typical soluble lysosomal proteins into the extracellular medium although their intracellular protein levels and proteolytic maturation were strongly decreased in KO cells generated in primary human fibroblast, U87MG, 293FT, HAP1, and SK-MEL-30 cells (fig. S5). In addition, we observed an increase in LC3B type II levels associated with autophagic membranes in cell lysates (fig. S5C). Autophagy markers or the accumulation of an autophagosome-specific dye were markedly elevated in LYSET and GNPTAB KO cells compared with WT cells under basal conditions and not further elevated by blocking lysosomal hydrolase activities with chloroquine (fig. S6A) or a combination of chloroquine and rapamycin (fig. S6B). This was expected because the content of autophagic vesicles is degraded by lysosomal hydrolases upon fusion with lysosomes (*19*). To more comprehensively assess the effects of LYSET knockout on a primary cell type, we used quantitative proteomic approaches in mouse embryonic fibroblasts (MEFs). We first generated C57BL/6J mice with deletions in *Lyset* by gene editing. We designed sgRNAs to excise a region in the second exon of *Lyset* resulting in two mouse lines with distinct out of frame deletion variants (of Δ184 and Δ199 nucleotides) (fig. S7, A to C and E). To generate mice with *Lyset* gene deletions (referred to as *Lyset* KO), mice were bred as compound heterozygotes (Δ184/Δ199) or homozygotes. We verified loss of Lyset protein expression in different tissues (fig. S7D). To investigate the extracellular proteome, we collected and concentrated serum-free conditioned medium from WT and *Lyset* KO MEFs. In parallel, we prepared cell lysates to determine the intracellular proteome. Using data independent acquisition (DIA) mass spectrometry (fig. S8A) (*20*), we detected and quantified more than 4000 proteins in the intracellular proteome and more than 1000 proteins in the secretome, showing a high correlation between replicates (fig. S8, B to E, and table S3). Only a small subset of proteins were differentially expressed in *Lyset* KO versus WT cells. Most of the proteins found in higher abundance in the secretome of *Lyset* KO MEFs were well-characterized luminal lysosomal proteins (indicated in red) whereas these proteins were depleted from the intracellular proteome (Fig. 2C and fig. S9A). The protein levels of two lysosomal enzymes known to traffic independently from M6P (Gba and Acp2) were unaffected (Fig. 2C), which we confirmed using specific activity assays (fig. S10). Moreover, membrane lysosomal proteins (indicated in blue) were unaffected (Fig. 2C). Similar results were obtained using parallel reaction monitoring (PRM), a targeted method that provides more sensitive quantification of a smaller subset of lysosomal proteins (fig. S9B) (*20*). Thus, LYSET deficiency results in a severe defect in lysosomal trafficking that is specific for M6P cargoes.

Key steps in lysosomal enzyme sorting include modification with M6P by GlcNAc-1-phosphotransferase in the Golgi apparatus and the subsequent binding to M6P-specific receptors that mediate the transport to the lysosome (*13*). To distinguish between an early defect in tagging or a later defect in M6P recognition, we used an unbiased proteomic approach to detect M6P modifications directly on glycoproteins isolated from WT cells and cells deficient in LYSET. This method, based on immobilized metal ion affinity chromatography (Fe^{3+}-IMAC), allows for enrichment of glycopeptides containing the negatively charged M6P modification followed by glycopeptide identification using mass spectrometry (fig. S11A) (*21*). In WT 293FT cells we readily identified glycopeptides containing M6P from canonical lysosomal enzymes (Fig. 2D, fig. S11B, and table S4). As expected, these M6P glycopeptides

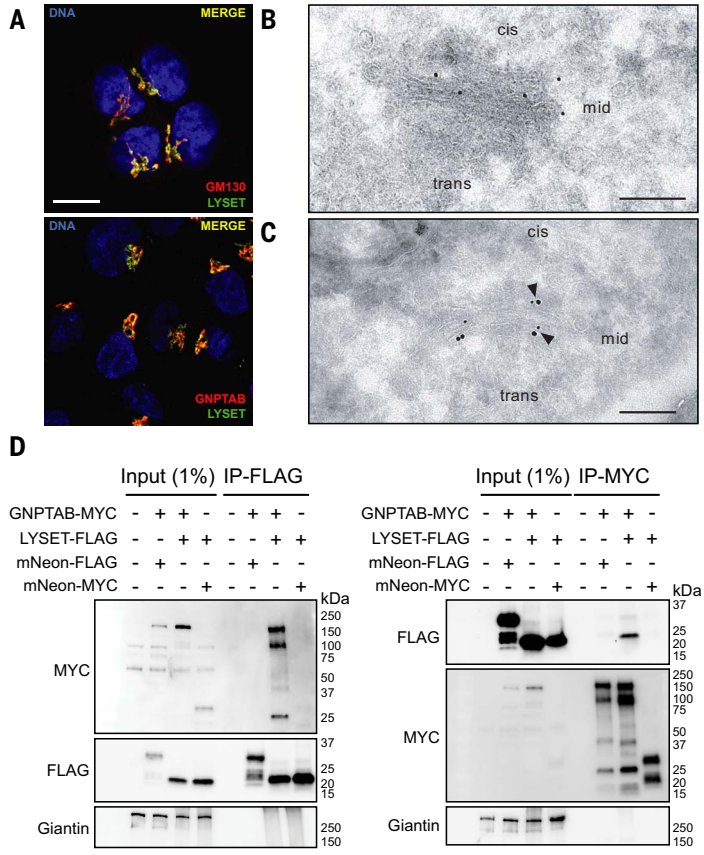

Fig. 3. LYSET binds to GNPTAB and colocalizes with GNPTAB/GNPTG in Golgi apparatus cisternae. (**A**) Immunofluorescence microscopy in HAP1 cells showing colocalization of LYSET with the cis-Golgi marker GM130 along with GNPTAB. Scale bar, 10 μm (**B**) Transmission electron microscopy (TEM) immunogold staining (15 nm gold) shows LYSET in Golgi cisternae of SK-MEL-30 WT cells using ultrathin sections. (**C**) TEM double immunogold staining on ultrathin sections for LYSET (15 nm gold) and GNPTG (10 nm gold) in the Golgi apparatus of SK-MEL-30 WT cells. Arrowheads indicate colocalization. Scale bar, 200 nm. (**D**) Immunoprecipitation (IP) on lysates of cells expressing epitope-tagged proteins using anti-FLAG (left panel) or anti-MYC (right panel) magnetic beads, followed by immunoblot analysis with indicated antibodies. Input lysates are also analyzed.

were absent in cells lacking GNPTAB. The LYSET KO cells displayed a similar absence of M6P-modified glycopeptides. This was confirmed in an orthologous assay using a single-chain M6P-specific antibody fragment (*22*). Lysates of 293FT and HAP1 cells devoid of LYSET showed a large decrease in M6P immunoreactive glycoproteins, comparable to decreases observed with GNPTAB KO and S1P KO cells (Fig. 2E and fig. S11C). Thus, LYSET is essential for an early step in lysosomal enzyme transport and the generation of the M6P modification.

LYSET binds to GNPTAB and regulates its function by mediating proper Golgi localization

LYSET is a small, poorly characterized protein containing two transmembrane domains. It colocalizes with GNPTAB and GNPTG in the Golgi apparatus (Fig. 3, A to C, and fig. S12, A to C). We performed immunoprecipitation (IP) followed by immunoblotting experiments to test whether LYSET interacts with GNPTAB. After coexpression of epitope-tagged LYSET and GNPTAB we detected GNPTAB-MYC in the LYSET-FLAG IP and LYSET-FLAG in the GNPTAB-MYC IP (Fig. 3D). These reciprocal co-IPs appeared to be specific as the endogenous Golgi protein Giantin was not detected and neither LYSET or GNPTAB was found in control IPs with epitope-tagged mNeonGreen. This interaction suggests that LYSET plays a role in modulating the function of the GlcNAc-1-phosphotransferase complex. Because pathogenic mutations in GNPTAB leading to mislocalization of the GlcNAc-1-phosphotransferase complex have been reported (*23*, *24*), we hypothesized that LYSET might function by retaining GNPTAB in the Golgi apparatus. We examined this by immunofluorescence analysis for endogenous GNPTAB and co-staining with antibodies for the Golgi apparatus (GM130) and lysosomes (LAMP2). The staining pattern in LYSET KO HAP1 cells was clearly distinct from WT cells. Whereas in WT cells GNPTAB was localized predominantly in the Golgi apparatus LYSET KO resulted in a loss of Golgi colocalization and a gain in localization to lysosomal structures (Fig. 4A). To investigate this further, we characterized the expression of the endogenous GlcNAc-1-phosphotransferase complex in subcellular fractions. We used sequential centrifugation to isolate a 20K fraction enriched in lysosomes and a 100K fraction enriched in ER/Golgi membranes (*25*). LYSET deficiency resulted in a near complete loss of endogenous GlcNAc-1-phosphotransferase α-subunit protein levels in the 100K fraction (Fig. 4B). This loss was post-transcriptional because GNPTAB mRNA levels did not substantially differ between WT and LYSET KO cells (fig. S13). Inhibition of proteasomal degradation with epoxomicin did not rescue expression of GNPTAB in LYSET KO cells (fig. S14, A and B). By contrast, preventing lysosomal degradation by blocking organellar acidification (bafilomycin A1) or by protease inhibition (PI) (E64d/leupeptin/pepstatin A) increased GNPTAB protein levels specifically in the lysosome-enriched 20K fraction (Fig. 4C and fig. S14, C to E). Moreover, following bafilomycin treatment we observed immunoreactive bands of higher electrophoretic mobility likely corresponding to partial cleavage products (Fig. 4C), which was also observed in magnetite-purified lysosomes (fig. S14F). These results suggest that GNPTAB is degraded in lysosomes. Immunofluorescence microscopy in LYSET KO cells revealed that most endogenous GNPTAB remained colocalized with a lysosomal marker upon treatment with both inhibitors (fig. S14, G and H). However, in bafilomycin—but not PI-treated—cells some GNPTAB colocalized with the Golgi apparatus (fig. S14, G and H). The latter could be due to a disturbance of the pH within the Golgi apparatus by bafilomycin that could lead to aberrant post Golgi trafficking (*26*). These data support a model in which LYSET interacts with GNPTAB and plays a major role in proper localization of GNPTAB in Golgi stacks. In the absence of LYSET, GNPTAB is mislocalized to the lysosomes where it is degraded.

LYSET's role in lysosomal transport provides a disease mechanism for a previously described genetic disorder

It has long been recognized that mutations in genes encoding the core components of lysosomal enzyme trafficking cause specific inherited syndromes including mucolipidosis II (MLII) in which defective GNPTAB mutations are etiological (*27*, *28*). Recently, biallelic LYSET mutations have been described in individuals from two families with a recessive genetic disorder with characteristics of mucopolysaccharidoses/mucolipidosis (*29*). However, the mechanistic basis upon which to link LYSET with the disease was tentative. Our results suggest that

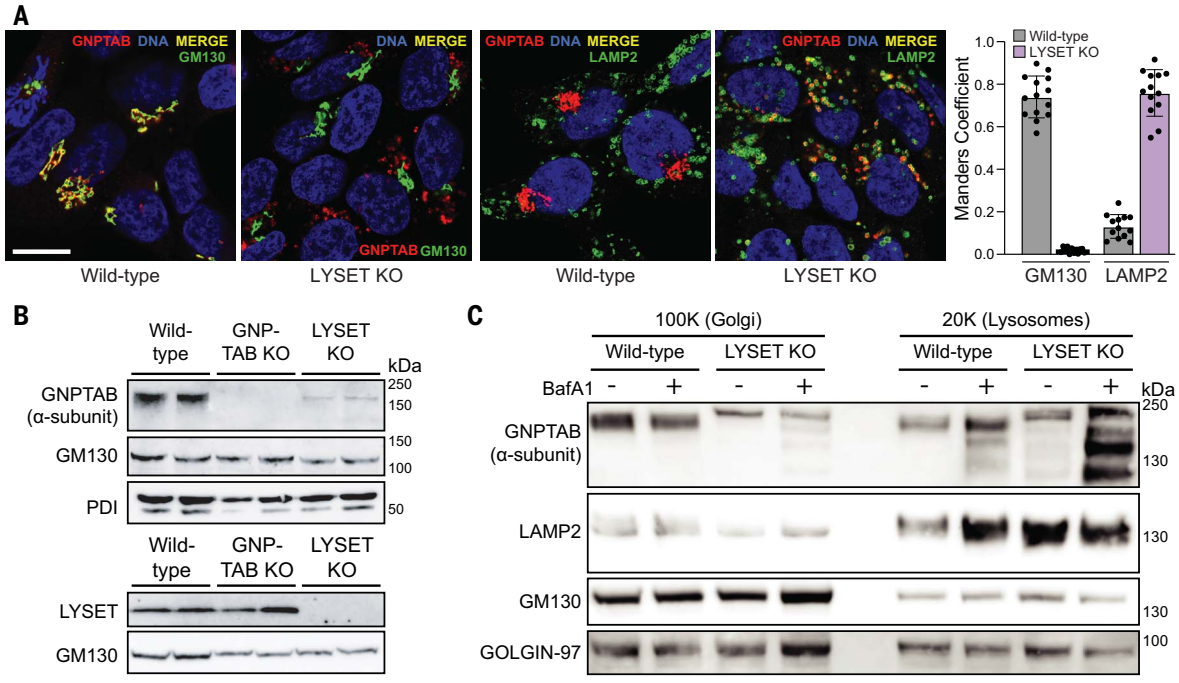

Fig. 4. LYSET KO triggers mislocalization of GNPTAB to the lysosome where it is degraded. (**A**) Colocalization of GNPTAB with GM130 and LAMP2 in WT and LYSET KO cells and Manders colocalization quantification. Colocalization analysis was performed on at least n = 12 separate micrograph images. Scale bar, 10 μm (**B**) Immunoblot analysis of GNPTAB in 100K-enriched ER/Golgi-fractions from WT, GNPTAB KO, and LYSET KO HAP1 cells. The antibody is specific for the α-subunit domain of GNPTAB. Golgi-marker (GM130) and ER-marker (PDI) proteins were used as loading controls. (**C**) Immunoblot analysis of 20K and 100K fractions from WT and LYSET KO HAP1 cells with or without bafilomycin A1 (BafA1) treatment. LAMP2, GM130 and GOLGIN-97 proteins were used as controls for preparation and loading.

defects in lysosomal protein sorting caused by LYSET deficiency might underlie this genetic disorder. Elevated serum level of lysosomal enzymes is a defining feature of MLII. The measurement of these enzymes in serum is used diagnostically to distinguish MLII from other metabolic diseases that cause similar clinical features (*28*). Compared with WT mice, serum from *Lyset* KO mice showed markedly higher enzyme activities of all tested lysosomal enzymes including α-mannosidase, β-hexosaminidase, α-L-fucosidase, and β-galactosidase (Fig. 5A). Furthermore, electron microscopy (EM) analysis of *Lyset* KO MEFs showed obvious morphological changes in lysosomes (Fig. 5B). Lysosomes with electron-dense material accumulated in the cytoplasm, another characteristic feature of lysosomal storage disorders (*28*). Quantitative analysis of EM images revealed that lysosomes were considerably larger and more numerous in *Lyset* KO MEFs although the cell area was not substantially different compared with WT cells (Fig. 5C and fig. S15, A and B). In line with this, aberrant lysosomes were also observed in human cells lacking LYSET (fig. S16). In addition, *Lyset* KO MEFs were resistant to infection by VSV-EBOV-GP, reinforcing our results in human cell lines (Fig. 5D and movies S9 and S10). Despite showing characteristic MLII phenotypes including increased lysosomal enzyme serum levels and storage materials in lysosomes, *Lyset* KO mice did not display obvious clinical symptoms as observed in human patients with LYSET mutations. Similarly, symptoms in the *Gnptab* KO mouse are less severe than in human MLII disease (*30*).

To link the human patient mutations in LYSET (*29*) directly to lysosomal protein sorting we first established that lentiviral complementation of WT LYSET (isoforms 1 and 2) could restore CTSB missorting and maturation in 293FT LYSET KO cells (fig. S17). Subsequently, we tested complementation by LYSET containing the Y72Ter or R45W pathogenic mutations (*29*). As controls we used WT LYSET as well as three nonsynonymous LYSET variants not associated with disease, which occur frequently in the population. R45W displayed slightly lower protein expression levels. As expected, Y72Ter was not detected because this frameshift mutation leads to a premature stop codon. While all controls corrected CTSB missorting, Y72Ter and R45W failed to do so (Fig. 6A). Similarly, R45W expression did not rescue the lysosomal storage defects observed using electron microscopy in LYSET KO cells (fig. S18). Moreover, the pathogenic allele R45W did not rescue the loss of endogenous GNPTAB in 100K fractions (Fig. 6B). Coimmunoprecipitation experiments showed a severe defect in R45W in binding with GNPTAB (Fig. 6C and fig. S19). Because R45W fails to rescue the lysosomal trafficking defect, these results suggest that the interaction of LYSET with GNPTAB is critical for GNPTAB function and that mutations in LYSET that affect this interaction can contribute to disease development. Thus, LYSET deficiency causes several defining features of mucolipidosis II and patient mutant alleles are compromised in the role of LYSET in M6P-dependent lysosomal protein sorting.

Conclusion

We establish LYSET as a Golgi-resident protein essential for M6P-mediated lysosomal protein trafficking. Our results support a model in which LYSET is essential for the activity of GlcNAc-1-phosphotransferase by binding to and retaining it in the Golgi apparatus. LYSET is relevant to human disease as patients with biallelic LYSET mutations suffer a genetic inherited disorder (*29*). Based on our elucidation of the role of LYSET in cell physiology, we propose that this disorder is similar to MLII. Because the clinical symptoms of mucolipidosis and mucopolysaccharidosis overlap and not all cases can be explained by mutations in known disease genes, *LYSET* sequencing may help to identify disease-causing mutations and, consequently, provide a more accurate diagnosis in patients. Furthermore, as an important component of lysosomal function, LYSET is essential for infection by diverse highly pathogenic

viruses that rely on endolysosomal activation by cathepsins.

Materials and methods summary

A detailed version of the materials and methods is provided in the supplementary materials. In brief, genome-scale CRISPR-Cas9 knockout libraries were generated in eHAP and U87MG cells. Libraries were infected with reovirus type 3D to select for a cell population containing mutations that confer resistance to viral infection. After genomic DNA isolation, PCR was used to amplify sequences encoding guide RNAs and their abundance was quantified using next generation sequencing. Statistical analysis was performed to identify and rank genes that were enriched in the selected population compared with the uninfected population.

LYSET KO mutations were introduced in different human cell lines using CRISPR-Cas9. Cells were infected with reovirus type 3D and viral infection was assessed using crystal violet assay, RT-qPCR and plaque forming assay. For infections with VSV pseudotyped with EBOV GP or SARS-CoV-2 S, viral entry was assayed using live cell imaging with an Incucyte system to monitor VSV-encoded GFP expression.

The endogenous expression of proteins involved in M6P lysosomal protein transport was determined in extracellular medium, intracellular lysates and subcellular organelle fractions in WT and KO cells using immunoblotting, lysosomal enzyme activity assays and mass-spectrometry. Binding between LYSET and GNPTAB was determined using coimmunoprecipitations from lysates of cells transfected with plasmids encoding epitope-tagged proteins.

All experiments involving mice were approved by Stanford's Institutional Animal Care and Use Committee. C57BL/6J zygotes were pronuclear injected with Cas9 RNPs targeting Lyset (Tmem251) with two synthetic gRNAs to introduce a frameshift mutation.

For electron microscopy, cells were fixed, osmicated, and Epon polymerized. Ultrathin sections (60 nm) were prepared and examined in an EM902 microscope. For postembedding immunogold labeling, ultrathin sections (60 nm) were prepared from cryoprotected cell pellets (2.3 M sucrose), collected on Carbon-Formvar-coated nickel grids, and incubated with one or two antibodies followed by protein A-coupled to colloidal gold particles. Images were acquired with a JEM- 2100Plus Transmission Electron Microscope.

For immunofluorescence, cells treated or not for 24 hours with lysosomal protease inhibitors (leupeptin, pepstatin A and E64d) or bafilomycin A1 were fixed with 4% PFA, blocked and

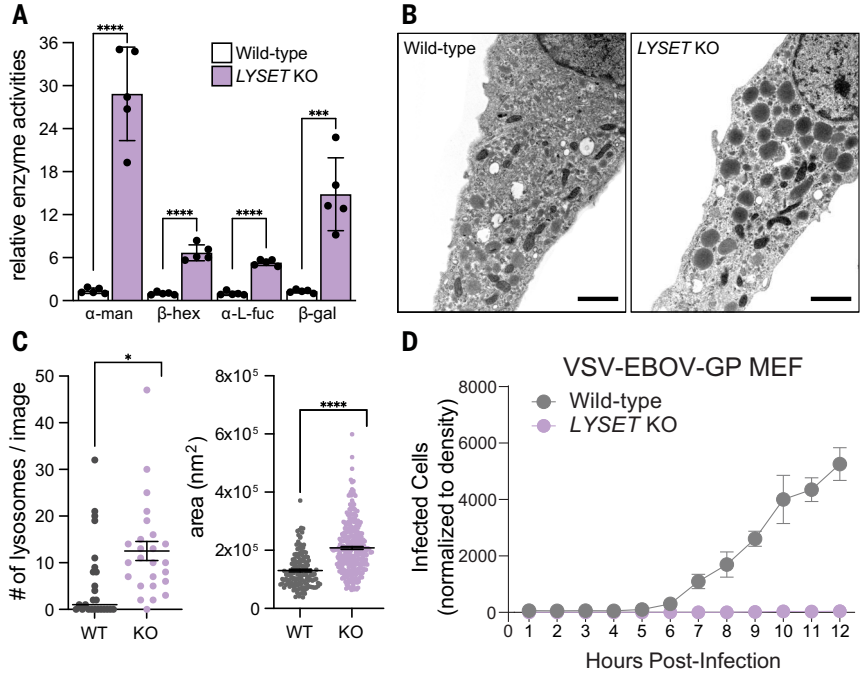

Fig. 5. Lyset KO mice display characteristics used to diagnose ML-II disease including elevated blood serum levels of lysosomal enzymes and aberrant lysosomes in isolated cells. (**A**) Relative enzyme activities of α-mannosidase (α-man), β-hexosaminidase (β-hex), α-L-fucosidase (α-L-fuc) and β-galactosidase (β-gal) from blood sera of adult WT and *Lyset* KO mice; WT activities set to 1; mean ± SD, $n = 5$ mice, ***$P < 0.001$, ****$P < 0.0001$, unpaired student's t-test (two-tailed). (**B**) Electron micrographs of WT and *Lyset* KO MEFs. Scale bar, 1 μm. (**C**) Numbers of lysosomes and areas counted for 25 independent images for WT and *Lyset* KO MEFs; mean ± SEM; unpaired, two-tailed student's t-test with Welch's correction; *$P < 0.05$, ****$P < 0.0001$. (**D**) Time course of VSV-EBOV-GP infection of WT and KO MEFs (mean ± SD, $n = 3$).

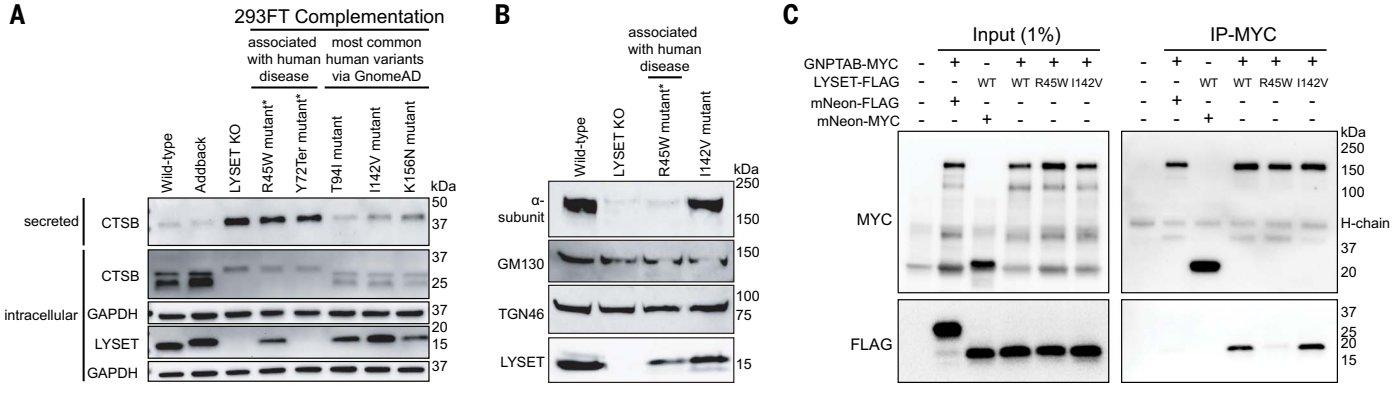

Fig. 6. Pathogenic LYSET mutations fail to restore lysosomal transport defects in LYSET KO cells. (**A**) Immunoblot of 293FT lysates or supernatants from LYSET KO cells complemented with WT LYSET (addback) or human variants. R45W and Y72Ter are patient-mutations (*22*); T94I, I142V, and K156N variants are not associated with disease. (**B**) Immunoblots of 100K-enriched Golgi/ER fractions from 293FT KO cells complemented with indicated LYSET alleles. (**C**) Immunoprecipitation (IP) on lysates of cells expressing epitope-tagged proteins using anti-MYC magnetic beads followed by immunoblot analysis with indicated antibodies.

permeabilized in BSA/saponin buffer followed by incubations with primary antibodies, Alexa Fluor-coupled secondary antibodies and Hoechst 33342. Images were acquired using a LSM880 confocal microscope equipped with an Airyscan detector. For in situ labeling of glucocerebrosidase (GBA) GBA inhibody MDW933 was used before fixation. BMV-109 probes were applied for live cell imaging of cysteine cathepsin activities on an Axiovert 200 M confocal microscope. Autophagic vacuole accumulation was visualized using the CYTO-ID Autophagy detection kit. All images were processed using ImageJ (https://imagej.nih.gov/ij/notes.html). The Manders colocalization coefficient was determined by means of the JACoP plug-in.

For mass-spectrometry, proteins were extracted from cell lysates and conditioned media by chloroform/methanol, digested by trypsin in the presence of RapiGest, and the concentration of desalted samples was determined using a peptide assay. For each sample, 1 μg of peptide was analyzed by UHPLC-MSMS using self-packed columns in combination with a Dionex Ultimate 3000 nano-UHPLC system coupled to an Orbitrap Fusion Lumos mass spectrometer. Data acquisition was performed using PRM, with a previously established assay for the analysis of lysosomal proteins, and data independent acquisition (DIA) for both sample types. Raw files were analyzed by Skyline (PRM) and Spectronaut (DIA) with determination of significantly regulated proteins based on fold-change and p/q-values. The mass spectrometry proteomics data have been deposited to the ProteomeXchange Consortium through the PRIDE partner repository with the dataset identifier PXD029609.

For glycoproteomics, cells were lysed and protein digestion was performed using an S-trap mini column protocol. Peptides were then enriched with immobilized metal affinity chromatography with iron-functionalized magnetic beads. Subsequently, peptide mixtures were separated over an EasySpray reversed phase LC column. The mobile phases were driven and controlled by a Dionex Ultimate 3000 RPLC nano system. An integrated loading pump was used to load peptides onto a trap column, which was put in line with the analytical column. Eluted peptides were analyzed on an Orbitrap Fusion Tribrid MS system. All data were searched with Byonic using the entire human proteome downloaded and an N-glycan database of 183 N-glycans that included M6P glycans. The mass spectrometry proteomics data have been deposited to the ProteomeXchange Consortium through the PRIDE partner repository with the dataset identifier PXD029746.

REFERENCES AND NOTES

1. J. Mercer, M. Schelhaas, A. Helenius, Virus entry by endocytosis. *Annu. Rev. Biochem.* **79**, 803–833 (2010). doi: 10.1146/annurev-biochem-060208-104626; pmid: 20196649
2. B. A. Mainou, T. S. Dermody, In search of cathepsins: How reovirus enters host cells. *DNA Cell Biol.* **31**, 1646–1649 (2012). doi: 10.1089/dna.2012.1868; pmid: 23134451
3. K. Chandran, N. J. Sullivan, U. Felbor, S. P. Whelan, J. M. Cunningham, Endosomal proteolysis of the Ebola virus glycoprotein is necessary for infection. *Science* **308**, 1643–1645 (2005). doi: 10.1126/science.1110656; pmid: 15831716
4. K. Shirato, M. Kawase, S. Matsuyama, Middle East respiratory syndrome coronavirus infection mediated by the transmembrane serine protease TMPRSS2. *J. Virol.* **87**, 12552–12561 (2013). doi: 10.1128/JVI.01890-13; pmid: 24027332
5. M. Hoffmann *et al.*, SARS-CoV-2 Cell Entry Depends on ACE2 and TMPRSS2 and Is Blocked by a Clinically Proven Protease Inhibitor. *Cell* **181**, 271–280.e8 (2020). doi: 10.1016/j.cell.2020.02.052; pmid: 32142651
6. G. Simmons *et al.*, Inhibitors of cathepsin L prevent severe acute respiratory syndrome coronavirus entry. *Proc. Natl. Acad. Sci. U.S.A.* **102**, 11876–11881 (2005). doi: 10.1073/pnas.0505577102; pmid: 16081529
7. J. G. Doench *et al.*, Optimized sgRNA design to maximize activity and minimize off-target effects of CRISPR-Cas9. *Nat. Biotechnol.* **34**, 184–191 (2016). doi: 10.1038/nbt.3437; pmid: 26780180
8. D. H. Ebert, J. Deussing, C. Peters, T. S. Dermody, Cathepsin L and cathepsin B mediate reovirus disassembly in murine fibroblast cells. *J. Biol. Chem.* **277**, 24609–24617 (2002). doi: 10.1074/jbc.M201107200; pmid: 11986312
9. L. Mach, Biosynthesis of lysosomal proteinases in health and disease. *Biol. Chem.* **383**, 751–756 (2002). doi: 10.1515/BC.2002.078; pmid: 12108539
10. S. Tiede *et al.*, Mucolipidosis II is caused by mutations in GNPTA encoding the alpha/beta GlcNAc-1-phosphotransferase. *Nat. Med.* **11**, 1109–1112 (2005). doi: 10.1038/nm1305; pmid: 16200072
11. A. Raas-Rothschild *et al.*, Molecular basis of variant pseudo-hurler polydystrophy (mucolipidosis IIIC). *J. Clin. Invest.* **105**, 673–681 (2000). doi: 10.1172/JCI5826; pmid: 10712439
12. K. Marschner, K. Kollmann, M. Schweizer, T. Braulke, S. Pohl, A key enzyme in the biogenesis of lysosomes is a protease that regulates cholesterol metabolism. *Science* **333**, 87–90 (2011). doi: 10.1126/science.1205677; pmid: 21719679
13. T. Braulke, J. S. Bonifacino, Sorting of lysosomal proteins. *Biochim. Biophys. Acta* **1793**, 605–614 (2009). doi: 10.1016/j.bbamcr.2008.10.016; pmid: 19046998
14. A. Takada *et al.*, A system for functional analysis of Ebola virus glycoprotein. *Proc. Natl. Acad. Sci. U.S.A.* **94**, 14764–14769 (1997). doi: 10.1073/pnas.94.26.14764; pmid: 9405687
15. X. Xie *et al.*, An Infectious cDNA Clone of SARS-CoV-2. *Cell Host Microbe* **27**, 841–848.e3 (2020). doi: 10.1016/j.chom.2020.04.004; pmid: 32289263
16. K. P. Y. Hui *et al.*, SARS-CoV-2 Omicron variant replication in human bronchus and lung ex vivo. *Nature* **603**, 715–720 (2022). doi: 10.1038/s41586-022-04479-6; pmid: 35104836
17. B. Meng *et al.*, Altered TMPRSS2 usage by SARS-CoV-2 Omicron impacts infectivity and fusogenicity. *Nature* **603**, 706–714 (2022). doi: 10.1038/s41586-022-04474-x; pmid: 35104837
18. M. Verdoes *et al.*, Improved quenched fluorescent probe for imaging of cysteine cathepsin activity. *J. Am. Chem. Soc.* **135**, 14726–14730 (2013). doi: 10.1021/ja4056068; pmid: 23971698
19. M. Boonen, E. van Meel, V. Oorschot, J. Klumperman, S. Kornfeld, Vacuolization of mucolipidosis type II mouse exocrine gland cells represents accumulation of autolysosomes. *Mol. Biol. Cell* **22**, 1135–1147 (2011). doi: 10.1091/mbc.e10-07-0584; pmid: 21325625
20. P. Mosen, A. Sanner, J. Singh, D. Winter, Targeted Quantification of the Lysosomal Proteome in Complex Samples. *Proteomes* **9**, 4 (2021). doi: 10.3390/proteomes9010004; pmid: 33530589
21. T. Čaval *et al.*, Targeted Analysis of Lysosomal Directed Proteins and Their Sites of Mannose-6-phosphate Modification. *Mol. Cell. Proteomics* **18**, 16–27 (2019). doi: 10.1074/mcp.RA118.000967; pmid: 30237200
22. S. Müller-Loennies, G. Galliciotti, K. Kollmann, M. Glatzel, T. Braulke, A novel single-chain antibody fragment for detection of mannose 6-phosphate-containing proteins: Application in mucolipidosis type II patients and mice. *Am. J. Pathol.* **177**, 240–247 (2010). doi: 10.2353/ajpath.2010.090954; pmid: 20472886
23. E. van Meel, Y. Qian, S. A. Kornfeld, Mislocalization of phosphotransferase as a cause of mucolipidosis III αβ. *Proc. Natl. Acad. Sci. U.S.A.* **111**, 3532–3537 (2014). doi: 10.1073/pnas.1401417111; pmid: 24550498
24. W. S. Lee, B. C. Jennings, B. Doray, S. Kornfeld, Disease-causing missense mutations within the N-terminal transmembrane domain of GlcNAc-1-phosphotransferase impair endoplasmic reticulum translocation or Golgi retention. *Hum. Mutat.* **41**, 1321–1328 (2020). doi: 10.1002/humu.24019; pmid: 32220096
25. J. M. Graham, Fractionation of Subcellular Organelles. *Curr. Protoc. Cell Biol.* **69**, cb0301s69 (2015). doi: 10.1002/humu.24019; pmid: 32220096
26. M. A. Axelsson *et al.*, Neutralization of pH in the Golgi apparatus causes redistribution of glycosyltransferases and changes in the O-glycosylation of mucins. *Glycobiology* **11**, 633–644 (2001). doi: 10.1093/glycob/11.8.633; pmid: 11479274
27. J. G. Leroy, R. I. Demars, Mutant enzymatic and cytological phenotypes in cultured human fibroblasts. *Science* **157**, 804–806 (1967). doi: 10.1126/science.157.3790.804; pmid: 17842782
28. S. A. Khan, S. C. Tomatsu, Mucolipidoses Overview: Past, Present, and Future. *Int. J. Mol. Sci.* **21**, 6812 (2020). doi: 10.3390/ijms21186812; pmid: 32957425
29. N. U. Ain *et al.*, Biallelic TMEM251 variants in patients with severe skeletal dysplasia and extreme short stature. *Hum. Mutat.* **42**, 89–101 (2021). doi: 10.1002/humu.24139; pmid: 33252156
30. C. M. Gelfman *et al.*, Mice lacking alpha/beta subunits of GlcNAc-1-phosphotransferase exhibit growth retardation, retinal degeneration, and secretory cell lesions. *Invest. Ophthalmol. Vis. Sci.* **48**, 5221–5228 (2007). doi: 10.1167/iovs.07-0452; pmid: 17962477

ACKNOWLEDGMENTS

The authors thank A. Dupzyk, B. Waldman, A. Johnson, and C. LaPointe for insightful comments. We thank M. Bassik and D. Monack for access to their respective Incucyte microscopes, E. Szpotowicz, C. Raithore, and J. Rehberg for technical assistance, and R. Hardt for support with DIA and PRM data analysis and visualization. We thank F. Seyfried, G. Dubberke, F. Koch-Nolte, and Institute of Immunology, UKE, Hamburg, for assistance with the production of mAb RG95-A96. We thank W. Palm for sharing unpublished data. Some images were created with BioRender.com. **Funding:** This work was funded in part by the National Institutes of Health (NIH) T32 AI007502 (to C.M.R.); NIH T32 GM007276 (to L.D.V.); NIH T32 AI007502 (to A.R.); NIH R01 AI140186 (to J.E.C.); NIH R01 AI141970 (to J.E.C.); NIH R01 AI130123 (to J.E.C.); NIH R01 GM058867 (to C.R.B.); NIH R01 AI134907 (to P.-Y.S); NIH K00CA21245 (to N.M.R.); Deutsche Forschungsgemeinschaft (DFG) CRC877 (to T.B. and M.S.); DFG FOR2625 TP7 (to P.R.M., D.W., and T.B.); DFG 240245660-SFB1129 (to R.B.); DFG 272983813-TRR 179 (to R.B.); Helmholtz Association's Initiative and Networking Fund KA1-Co-02 "COVIPA" (to R.B.); Burroughs Wellcome Fund Investigators in the Pathogenesis of Infectious Disease (to J.E.C.); Stanford ChEM-H Innovative Medicines Accelerator (to J.E.C); Sealy Smith Foundation (to P.-Y.S); Kleberg Foundation (to P.-Y.S); John S. Dunn Foundation (to P.-Y.S); Amon G. Carter Foundation (to P.-Y.S); Gillson Longenbaugh Foundation (to P.-Y.S); and Summerfield Robert Foundation (to P.-Y.S). **Author contributions:** C.M.R., S.J., and W.Q. were responsible for design and execution of the experiments, data analysis, and manuscript preparation. C.M.R. designed and performed the U87MG and eHAP CRISPR screens with ReoT3D. C.M.R., W.Q., and Y.S.O. generated the U87MG mutagenized library. C.M.R. generated the eHAP mutagenized library. W.Q. performed MAGeCK analyses. J.C.W., C.M.R., and M.B. designed and executed experiments with the BMV-109 pan-cathepsin probe. N.M.R., R.A.F., and C.R.B. designed, collected, and analyzed the $Fe3^{+}$-IMAC-based proteomics data. P.R.M. and D.W. designed, collected, and analyzed the MEF intracellular and secreted proteomics data. C.M.N. and C.M.R. were responsible for the in vivo mouse experiments and analysis. C.M.R. and J.R.Z. rescued and sequenced VSV-EBOV-GP. C.M.R., L.D.V., and W.Q. cloned all LYSET expression plasmids. J.R.Z. performed the time-course microscopy (Incucyte) infection experiments. C.M.R. generated Vero E6 ACE2-Flag and Vero E6 TMPRSS2-TwinStrep expressing cell lines. J.R.Z. rescued and sequenced VSV-SARS-CoV-2-S and VSV-SARS-CoV-2*. M.S. performed electron microscopy experiments and analysis. C.M.R., S.J., L.D.V., M.K., and W.Q. performed immunoblotting experiments. C.M.R., L.D.V., and W.Q. generated the (non-commercially purchased) isogenic knockout, pooled knockout, and complemented cell lines. S.J. and C.E.P. performed confocal immunofluorescence experiments. X.X. and P.-Y.S. provided stocks of SARS-CoV-2-mNeon. A.R. performed SARS-CoV-2-mNeon infections and flow cytometry supervised by C.A.B. R.B. provided A549-ACE2 cells. A.P. provided Huh7.5.1-ACE2/TMPRSS2 cells. J.E.C. and T.B. designed and

supervised the research, interpreted the data, and prepared the manuscript. All authors provided comments for the manuscript and agreed on the final version. **Competing interests:** J.E.C. consulted for Janssen BioPharma on topics unrelated to this study. C.R.B. is a cofounder and Scientific Advisory Board member of Lycia Therapeutics, Palleon Pharmaceuticals, Enable Bioscience, Redwood Biosciences (a subsidiary of Catalent) and InterVenn Biosciences. C.A.B. reports compensation for consulting and/or SAB membership from Catamaran Bio, DeepCell Inc., Immunebridge, Sangamo Therapeutics, Bicycle Tx, and Revelation Biosciences on topics unrelated to this study. The remaining authors declare no competing interests. **Data and materials availability:** All data presented are available in the main text or the supplementary materials. FASTQ files for CRISPR screens are available at ArrayExpress (Accession# E-MTAB-11158). Acquired glycoproteomics data are available at ProteomeXchange with identifier PXD029746 and DIA and PRM data with identifier PXD029609. Cell lines and LYSET knockout mice generated in the laboratory of J.E.C. are available upon request to J.E.C. under a material transfer agreement from Stanford University. Huh7.5.1 derivatives require an additional material transfer agreement from Apath.

SUPPLEMENTARY MATERIALS

science.org/doi/10.1126/science.abn5648
Materials and Methods
Figs. S1 to S19
Tables S1 to S6
References (*31*–*70*)
Movies S1 to S10

View/request a protocol for this paper from Bio-protocol.

Submitted 5 December 2021; resubmitted 20 June 2022
Accepted 26 August 2022
10.1126/science.abn5648

The human disease gene LYSET is essential for lysosomal enzyme transport and viral infection

Christopher M. Richards, Sabrina Jabs, Wenjie Qiao, Lauren D. Varanese, Michaela Schweizer, Peter R. Mosen, Nicholas M. Riley, Malte Klssendorf, James R. Zengel, Ryan A. Flynn, Arjun Rustagi, John C. Widen, Christine E. Peters, Yaw Shin Ooi, Xuping Xie, Pei-Yong Shi, Ralf Bartenschlager, Andreas S. Puschnik, Matthew Bogyo, Carolyn R. Bertozzi, Catherine A. Blish, Dominic Winter, Claude M. Nagamine, Thomas Braulke, and Jan E. Carette

Science, **378** (6615), eabn5648.
DOI: 10.1126/science.abn5648

LYSET helps load lysosomes

Lysosomes are major degradative compartments within the cell, and their dysfunction results in both rare and common disorders. Certain viruses, including severe acute respiratory syndrome coronavirus 2 (SARS-CoV-2), hijack lysosomes to gain entry into the cell and start their destructive infection cycle. Richards *et al*. identified a small protein named LYSET that is critical for proper lysosomal function. In cells lacking LYSET, the trafficking of enzymes to the lysosomes was severely disrupted resulting in the accumulation of undigested material in the lysosome. Independently, Pechincha *et al*. identified LYSET as being selectively essential when cells feed on extracellular proteins. Cancer cells commonly rely on extracellular proteins to provide amino acids. LYSET helped to anchor *N*-acetylglucosamine-1-phosphotransferase in Golgi membranes for tagging enzymes with the lysosomal trafficking signal mannose-6-phosphate. Without LYSET, lysosomes were depleted of catabolic enzymes, losing their ability to digest extracellular proteins. —SMH